

Supplemental Data

Data S1: Additional Hi-C contact matrices relevant to main findings, Related to Figures 2, 3, 4, 5, and 6.

Data S1, I: Elimination of loop domains after cohesin loss

(A) An example region from Figure 2A shown at different color scales: contact maps from untreated cells on top and maps from auxin treated cells on the bottom. The lack of visible loop domain structure is not a result of color scale choice; there is no residual loop domain structure.

(B) Another example region from Figure 2A shown at different color scales; again there is no residual loop domain structure.

(C-G) Additional examples of complete elimination of loop domains after auxin treatment and degradation of cohesin. (C: chr10: 61.25-62.7 Mb; D: chr16: 77.1-78.2 Mb; E: chr9: 74.3-75.6 Mb; F: chr20: 49.4-50.5 Mb; G: chr15:80.6-81.8 Mb).

(H) To assure that the disappearance of loop domains after cohesin degradation did not arise as a result of cell cycle abnormalities, we performed Hi-C on cells that were synchronized and arrested at the G1/S boundary before and during auxin treatment. Here, we show an example of a loop domain (chr10: 16.7-17.5 Mb) that is present in our maps from G1/S-arrested cells and lost after auxin treatment.

(I-L) Additional examples of loop domains present in G1/S-arrested cells and lost after auxin treatment. (I: chr16: 19.4-20.1 Mb; J: chr13: 85.1-86.7 Mb; K: chr2: 121.2-122.1 Mb; L: chr9: 89.8-90.5 Mb).

Data S1, II: Variation in loop domain recovery across the genome

(A) Three examples of regions containing fast loop domains (1st row: chr11:34.45-35.1Mb; 2nd row: chr12:93.6-94.7Mb; 3rd row: chr12:64-64.9Mb) are shown, along with ChIP-Seq tracks (from auxin-treated cells) for NIPBL, H3K4me1, H3K4me3, and H3K27Ac. For fast loop domains, reformation is apparent by 20-40 minutes after auxin withdrawal, and enrichment for NIPBL, H3K4me1, H3K4me3, and H3K27Ac is observed.

(B) Three examples of regions containing slow loop domains (1st row: chr4:82.1-83.4Mb; 2nd row: chr3:63.15-64Mb; 3rd row: chr20:16.6-17.6Mb) are shown. For slow loop domains, reformation is not seen until 3 hours after auxin withdrawal and no enrichment for NIPBL, H3K4me1, H3K4me3, or H3K27Ac is observed.

Data S1, III: Comparison of compartment patterns before and after cohesin loss

(A,B) Examples (A: chr10:59.3-67Mb and B: chr2:153.6-163.15Mb) showing that the loss of cohesin-associated loops after auxin treatment results in increased fine-scale compartmentalization. Top: Sliding correlation scores; valleys imply strong differences in long-range contact pattern observed at a locus as compared to neighboring loci, indicating a change in compartment (STAR Methods). Middle: Observed contact matrices. Bottom: Pearson's correlation maps for the local region shown (STAR Methods). Deeper valleys in the sliding correlation score and increased plaid patterning in the observed and Pearson's correlation maps indicate strengthened fine-scale compartment interactions after auxin treatment. Blowouts: loss of a loop domain results in strengthening of a compartment boundary spanned by the loop. Blown-out regions are indicated on zoomed out maps for both the observed (black upper triangle) and Pearson's correlation maps (white rectangle). Observed and Pearson's correlation maps are both shown at 25kb resolution for the zoomed out matrices and 10kb and 25kb resolution respectively for the blown-out matrices.

Data S1, IV: Examples of cohesin-independent links

(A) Examples of a network of intrachromosomal cohesin-independent links between superenhancers on chr3. H3K27 acetylation does not change with auxin treatment, but cohesin-independent links are significantly strengthened upon treatment.

(B) Examples of a network of intra- and interchromosomal cohesin-independent links between superenhancers on chr7, chr6, chr4, and chr2. H3K27 acetylation does not change with auxin treatment, but cohesin-independent links are significantly strengthened upon treatment.

Data S1, V: A large cohesin-independent clique across an auxin withdrawal time course

(A-F) The interactions between 17 cohesin-independent loop anchors spread across 8 chromosomes are shown along an auxin withdrawal time course (A: 6hr auxin treatment; B: 20min withdrawal of auxin; C: 40min withdrawal of auxin; D: 60 min withdrawal of auxin; E: 180 min withdrawal of auxin; F: no auxin treatment). Each matrix shows a 2 Mb by 2 Mb matrix centered on the respective anchors. Intrachromosomal interactions are shown at 25kb resolution with a maximum intensity of 50 reads (auxin treated and untreated maps) or 13 reads (20, 40, 60, 180 min withdrawal maps); interchromosomal interactions are shown at 100kb resolution with a maximum intensity of 20 reads (auxin treated and untreated maps) or 5 reads (20, 40, 60, 180 min withdrawal maps). Cohesin-independent links are rapidly weakened and lost upon withdrawal of auxin.

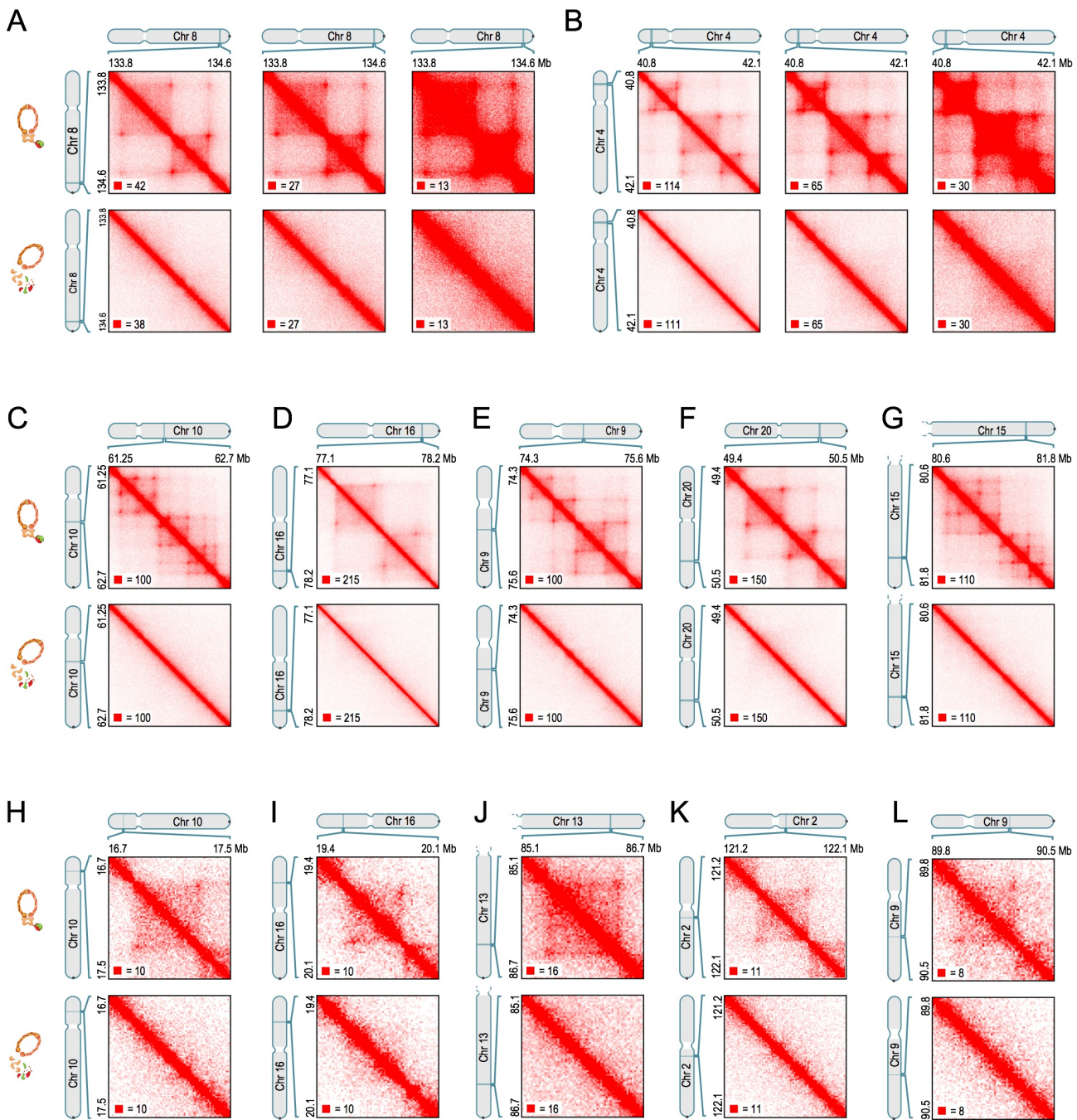
Data S1, VI: Simulations of extrusion and compartmentalization

(A) We use loop extrusion and compartmentalization to simulate a 2.1 Mb region on chromosome 3 in HCT-116 RAD21-mAC cells before (left) and after (right) auxin treatment. SMC1 ChIP-Seq signals are normalized and converted into binding probabilities for the simulated extrusion complex. Each peak is assigned a forward (green) or reverse (red) orientation based on the corresponding CTCF motif. Hi-C contact patterns in the treated map were used to determine the positions of compartment intervals (red and blue). The simulations yield an ensemble of polymer configurations. We show contact maps from the simulated ensemble (top) and from the corresponding Hi-C experiments (bottom). The simulations accurately capture the positions of loops and domains, as well as the loss of loop domains after the depletion of cohesin. In addition, our simulation accurately captures compartmentalization patterns seen before and after auxin treatment. Notably, one of the loop domains spans multiple compartment intervals; the loci between the boundary of one of the compartment intervals and the loop anchor are highlighted (grey).

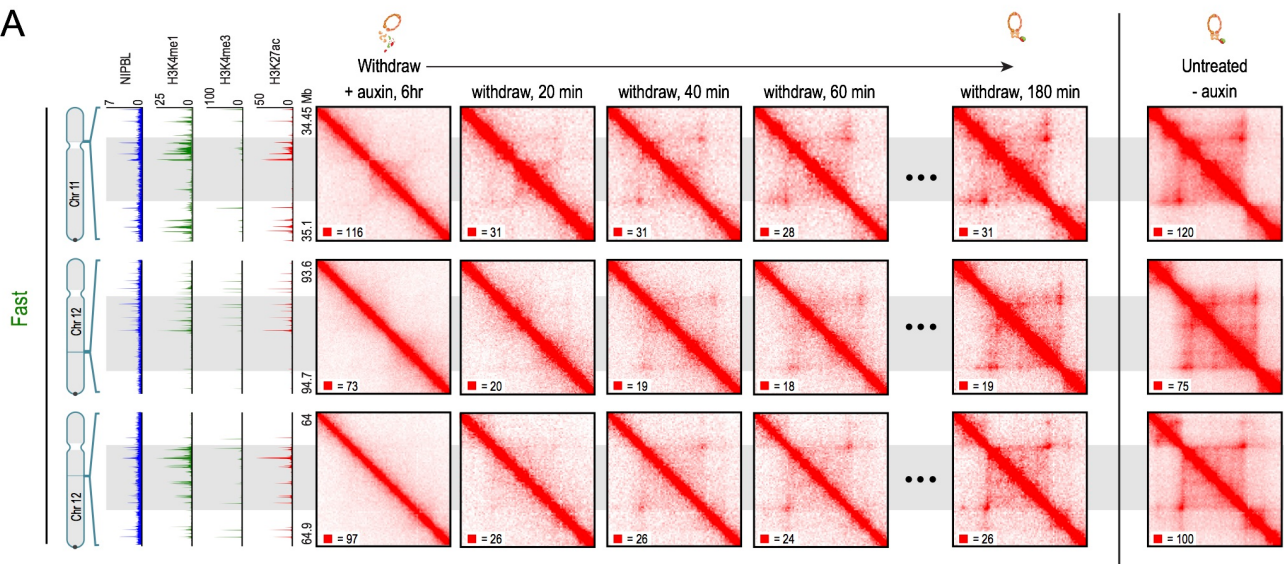
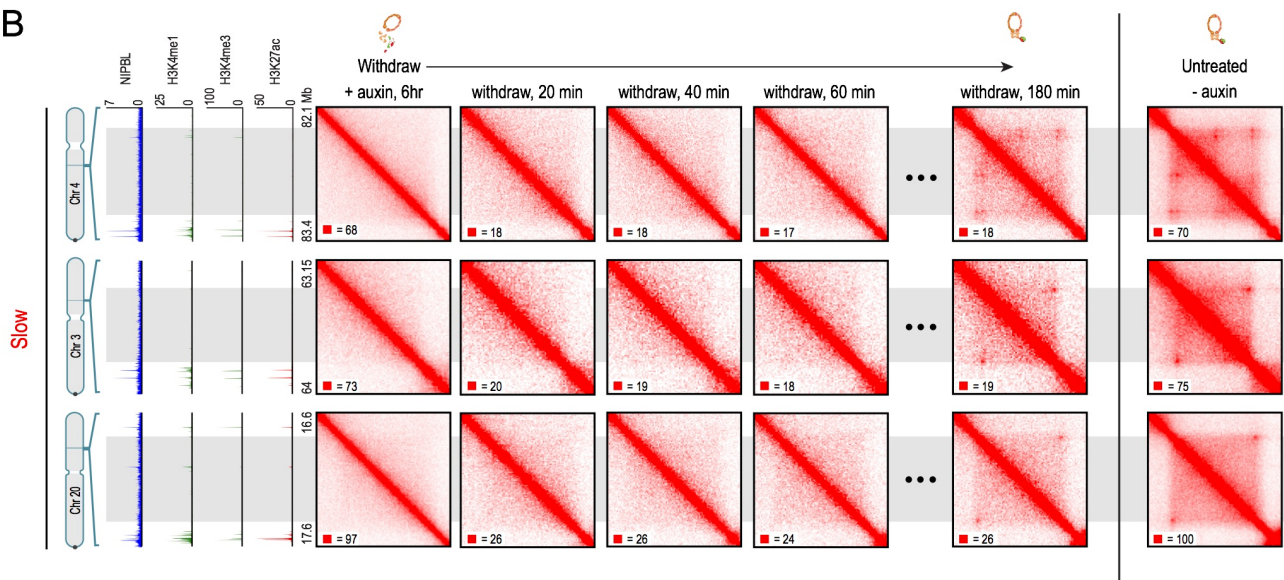
(B) Examples of globules from simulations of compartmentalization with extrusion (left) and without (right). Notably, the globule without extrusion shows stronger segregation of compartment types.

(C) Simulation of loop extrusion and compartmentalization in a 2.525 Mb region on chromosome 5 in HCT-116 RAD21mAC cells before (left) and after (right) auxin treatment. Compartment states were assigned either using an automated classification based on ChIP-Seq input data (top row), or a hand annotated compartment track (middle row). Notably, one of the loop domains spans multiple compartment intervals; the loci between the boundary of one of the compartment intervals and the loop anchor are highlighted (grey). Real Hi-C data is shown in the bottom row.

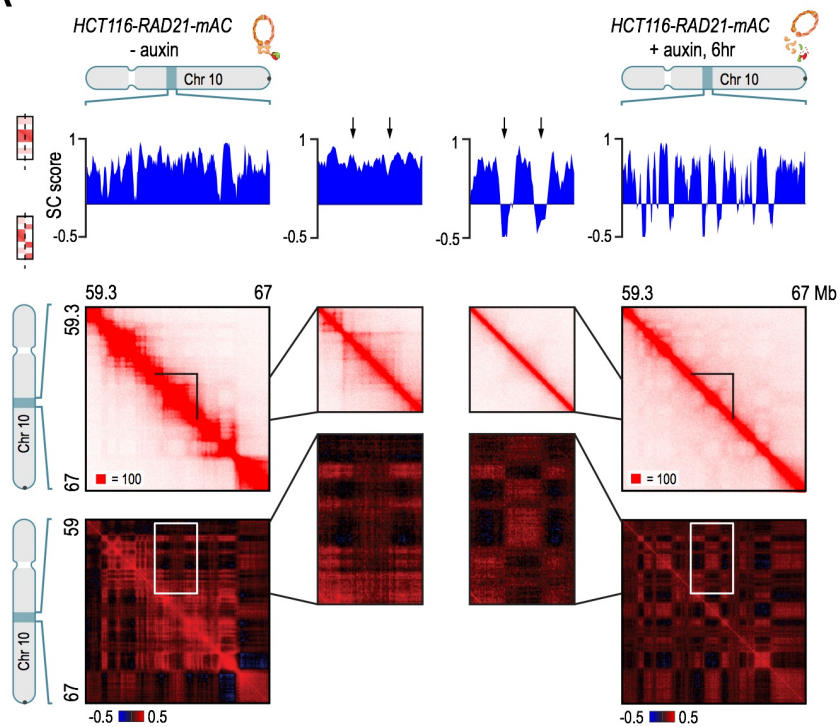
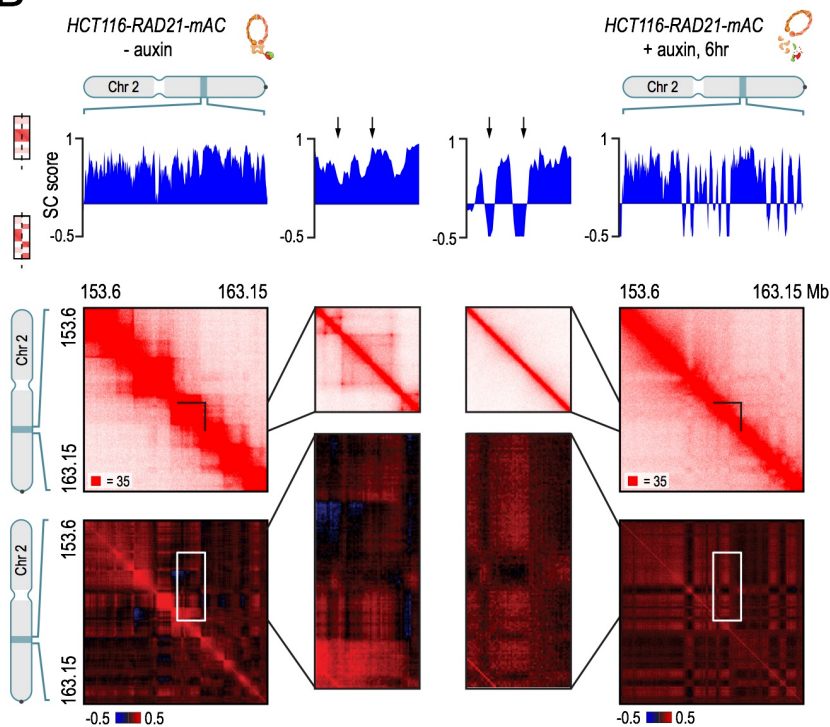
(D) Simulations as in (C), for another region (chr4:20-24Mb). As in (C), simulations using an automated annotation of compartment state are shown in the top row, and simulations using a hand annotation are shown in the middle row. Real Hi-C data is shown in the bottom row.



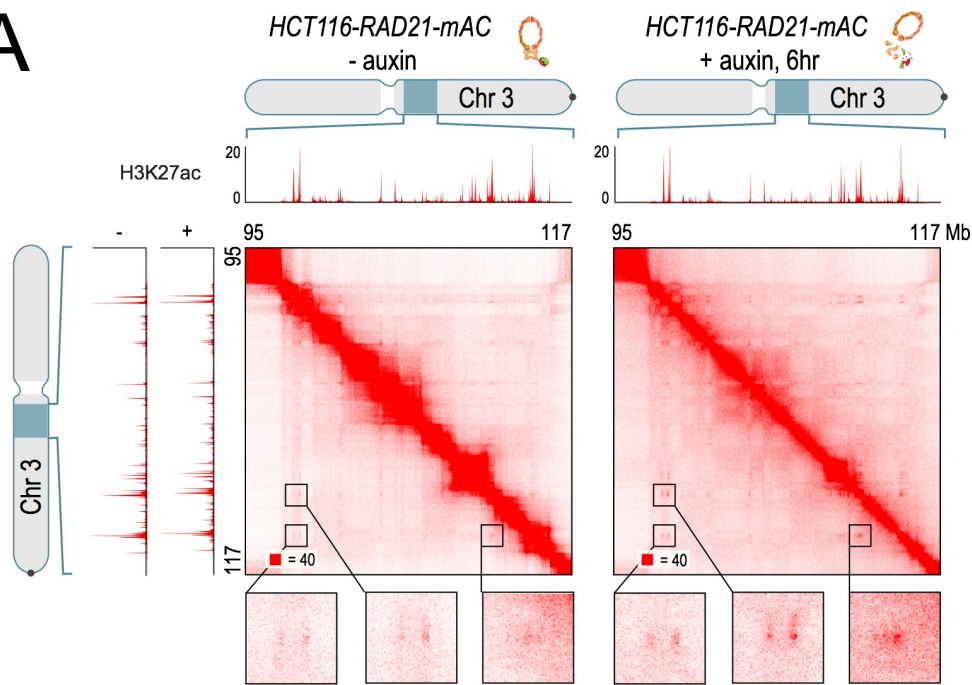
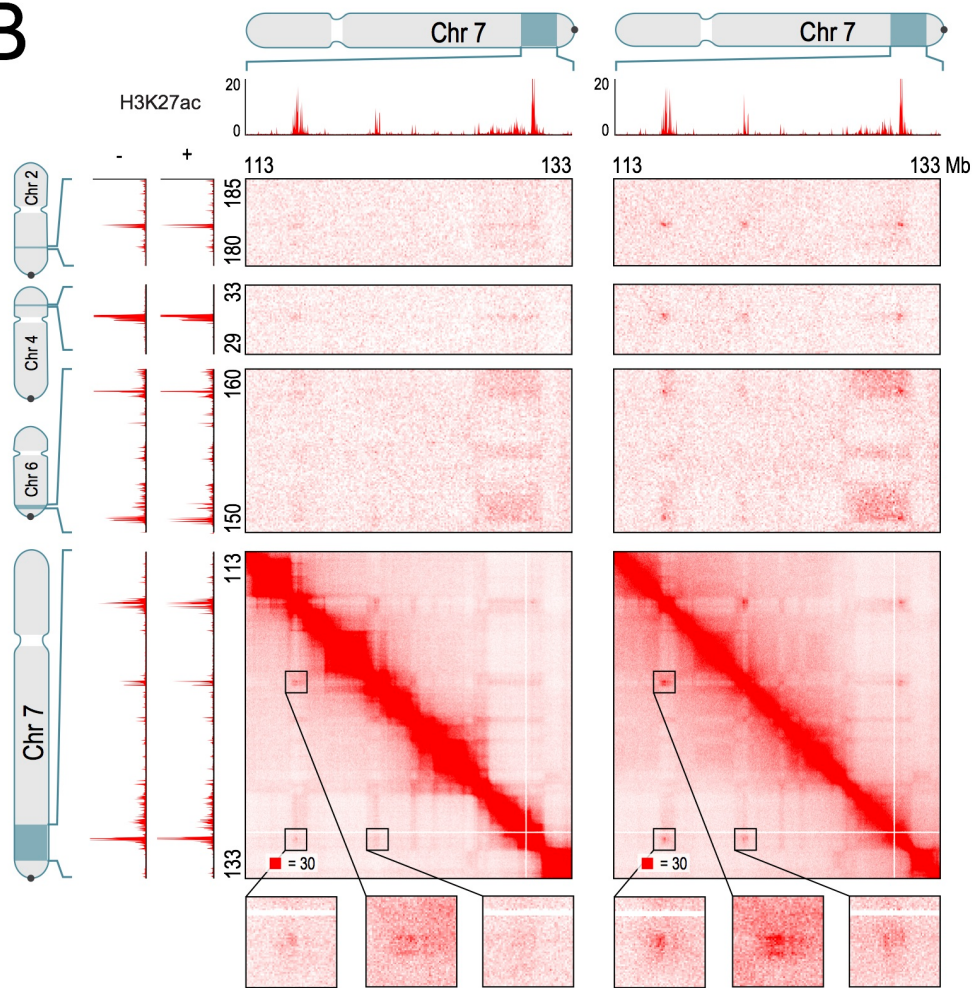
Data S1, I: Elimination of loop domains after cohesin loss

A**B**

Data S1, II: Variation in loop domain recovery across the genome

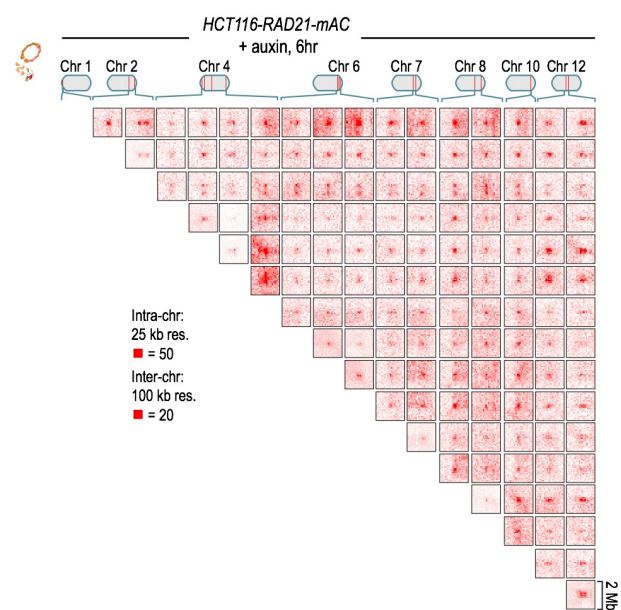
A**B**

Data S1, III: Comparison of compartment patterns before and after cohesin loss

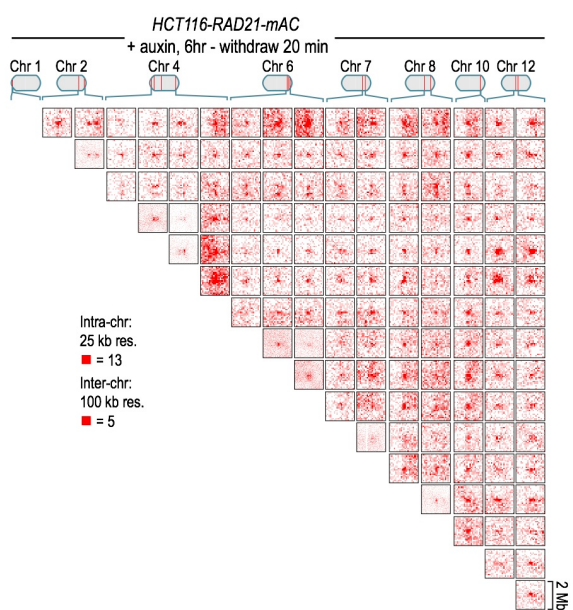
A**B**

Data S1, IV: Examples of cohesin-independent links

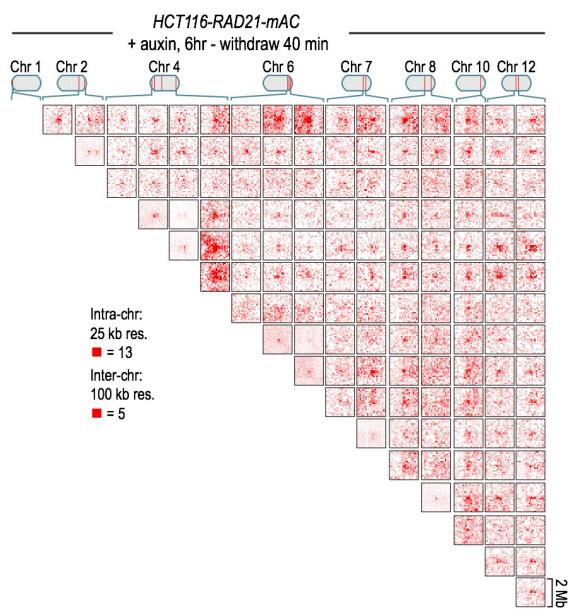
A



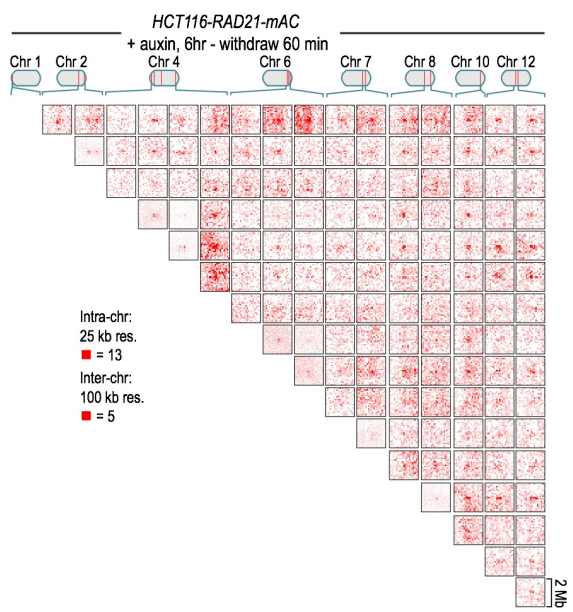
B



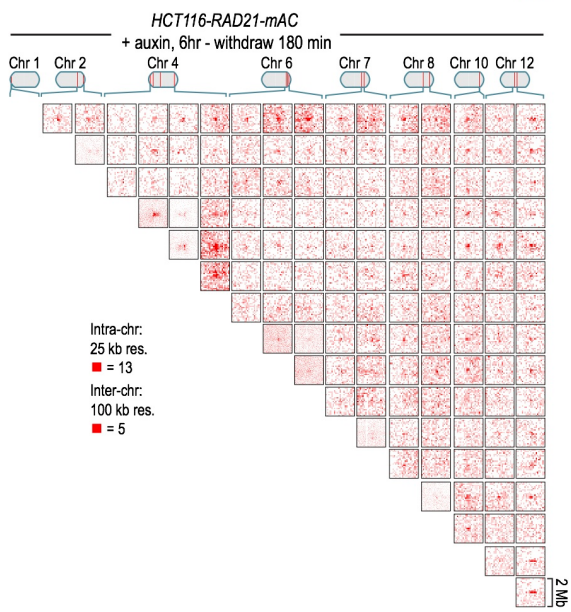
C



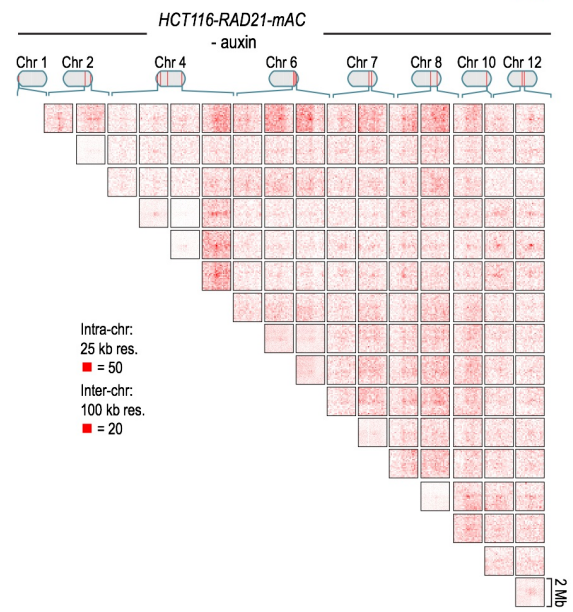
D



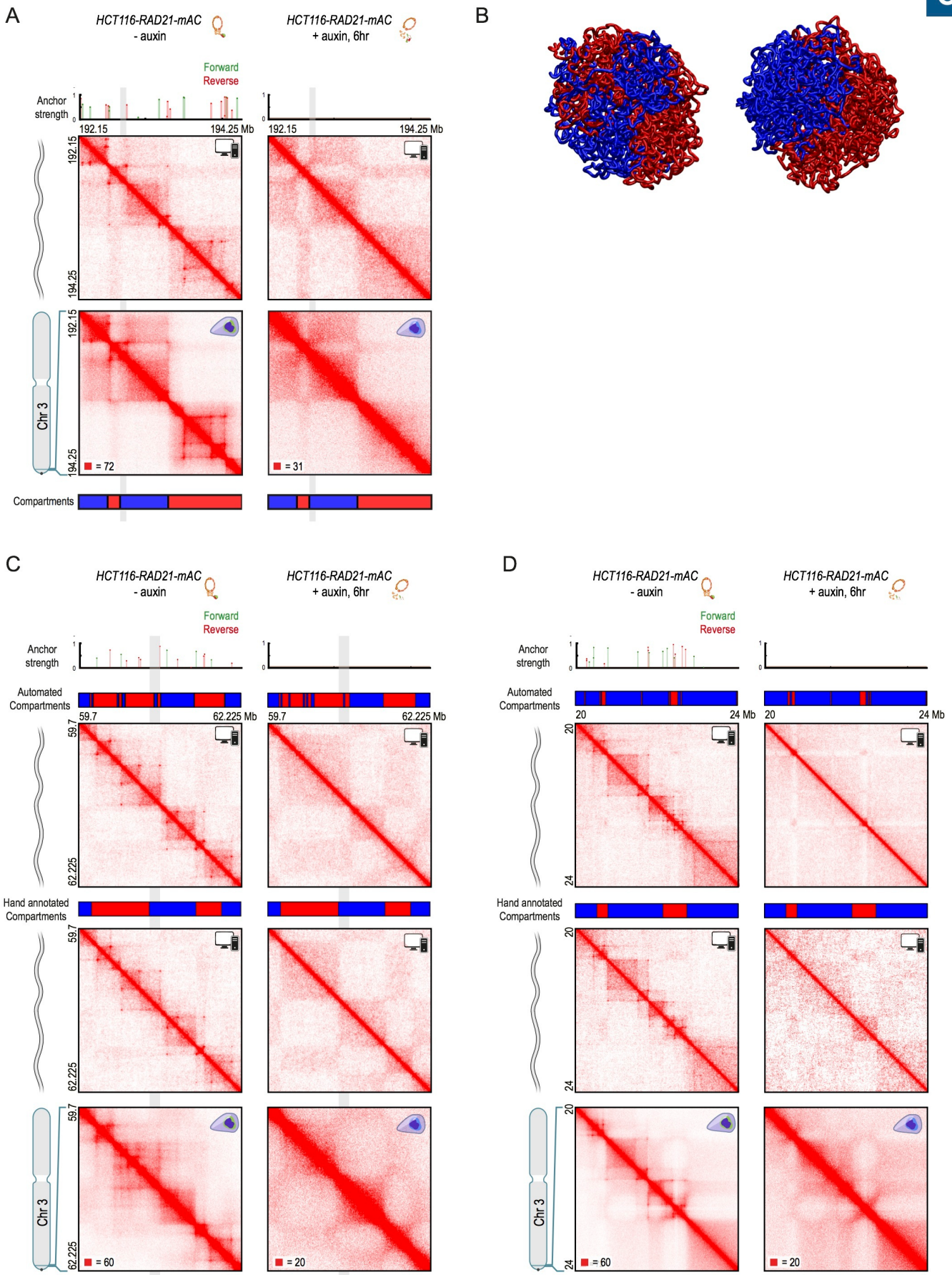
E



F



Data S1.V: A large cohesin-independent clique across an auxin withdrawal timecourse



Data S1, VI: Simulations of extrusion and compartmentalization